Geophysical Prospecting

EAGE EUROPEAN ASSOCIATION OF GEOSCIENTISTS & ENGINEERS

Geophysical Prospecting, 2012, **60**, 29–48 doi: 10.1111/j.1365-2478.2011.00964.x

Elastic wave mode separation for tilted transverse isotropic media

Jia Yan*‡ and Paul Sava

Center for Wave Phenomena, Colorado School of Mines, Department of Geophysics, 1500 Illinois St., Golden, CO 80401, USA

Received April 2010, revision accepted February 2011

ABSTRACT

Seismic waves propagate through the earth as a superposition of different wave modes. Seismic imaging in areas characterized by complex geology requires techniques based on accurate reconstruction of the seismic wavefields. A crucial component of the methods in this category, collectively known as wave-equation migration, is the imaging condition that extracts information about the discontinuities of physical properties from the reconstructed wavefields at every location in space. Conventional acoustic migration techniques image a scalar wavefield representing the P-wave mode, in contrast to elastic migration techniques, which image a vector wavefield representing both the P- and S-waves. For elastic imaging, it is desirable that the reconstructed vector fields are decomposed into pure wave modes, such that the imaging condition produces interpretable images, characterizing, for example, PP or PS reflectivity. In anisotropic media, wave mode separation can be achieved by projection of the reconstructed vector fields on the polarization vectors characterizing various wave modes. For heterogeneous media, because polarization directions change with position, wave mode separation needs to be implemented using space-domain filters. For transversely isotropic media with a tilted symmetry axis, the polarization vectors depend on the elastic material parameters, including the tilt angles. Using these parameters, we separate the wave modes by constructing nine filters corresponding to the nine Cartesian components of the three polarization directions at every grid point. Since the S polarization vectors in transverse isotropic media are not defined in the singular directions, e.g., along the symmetry axes, we construct these vectors by exploiting the orthogonality between the SV and SH polarization vectors, as well as their orthogonality with the P polarization vector. This procedure allows one to separate all three modes, with better preserved P-wave amplitudes than S-wave amplitudes. Realistic synthetic examples show that this wave mode separation is effective for both 2D and 3D models with strong heterogeneity and anisotropy.

Keywords: Anisotropy, Symmetry-axis plane, Wave mode.

INTRODUCTION

Although acoustic migration is currently the most common procedure for seismic imaging, imaging with multicomponent data has been recognized to have advantages in seeing through gas-charged sediments and in structural and near-surface imaging (Stewart *et al.* 2003). Two options are available for elastic imaging: 1) one can separate wave modes at the surface and image with the separated PP and PS data using acoustic migration tools (Sun *et al.* 2004), or 2) one can extrapolate the recorded multicomponent data and image with the reconstructed elastic wavefields by applying an imaging

*E-mail: jia.yan@exxonmobil.com
‡Now at ExxonMobil Upstream Research Company, Houston, TX 77027, USA.

© 2011 European Association of Geoscientists & Engineers

condition to wave modes separated in the vicinity of the image points (Yan and Sava 2008). The first approach benefits from the simplicity of imaging with scalar waves but it is based on the assumption that P- and S-modes can be successfully separated on the recording surface, which is difficult for complicated datasets. Plus, imaging with separated data also requires good single-mode propagators, which is more difficult for anisotropic media (Fowler, Du and Fletcher 2010; Zhang and Zhang 2009). The second approach reconstructs elastic wavefields in the subsurface, thus capturing all possible wave mode transmissions and reflections, although it increases the computational cost in elastic wavefield modelling. In addition, the elastic migration technique requires wave mode separation before the application of an imaging condition to avoid crosstalk between different wave modes.

In isotropic media, the P- and S-modes (shear waves do not split in isotropic media) can easily be separated by taking the divergence and curl of the elastic wavefield (Aki and Richards 2002). This procedure is effective in homogeneous as well as heterogeneous media. For isotropic media, in the far-field, P- and S-waves are polarized parallel and perpendicular to the wave vectors, respectively. The polarization directions of the P- and S-waves thus only depend on the wave propagation direction and are not altered by the medium. Therefore, the wave mode separators are invariant with space and divergence and curl can always be used to separate compressional (scalar) and shear (vector) wave modes.

However, divergence and curl do not fully separate wave-modes in anisotropic media, because P- and S-waves are not generally polarized parallel and perpendicular to the wave vectors. Dellinger and Etgen (1990) separate wave-modes in homogeneous vertically transversely isotropic (VTI) media by projecting the vector wavefields onto the polarization vectors of each mode. In VTI media, the polarization vectors of P- and SV-waves depend on the anisotropy parameters ϵ and δ (Thomsen 1986) and are spatially-varying when the medium is inhomogeneous. Therefore, Yan and Sava (2009) separate wave modes in heterogeneous VTI media by filtering the wavefields with spatially varying separators in the space domain and show that separation is effective even for complex geology with high heterogeneity.

However, VTI models are suitable only for limited geological settings with horizontal layering. Case studies have shown that TTI transversely isotropic with a tilted symmetry axis) models better represent complex geologies like thrusts and fold belts, e.g., the Canadian Foothills (Godfrey 1991). Using the VTI assumption to image structures characterized by TTI (tilted transverse isotropic) anisotropy introduces both kinematic and dynamical errors in migrated images. For example, Vestrum *et al.* (1999), Isaac and Lawyer (1999) and Behera and Tsvankin (2009) show that seismic structures can be mispositioned if isotropy, or even VTI anisotropy, is assumed when the medium above the imaging targets is TTI. To carry out elastic wave-equation migration for TTI models and apply the imaging condition that cross-correlates the separated wave modes, the wave mode separation algorithm needs to be adapted to TTI media. For sedimentary layers bent under geological forces, TTI migration models usually incorporate locally varying tilts and the local symmetry axes can be conveniently assumed to be orthogonal to the reflectors throughout the model (Charles *et al.* 2008; Alkhalifah and Sava 2010) (The industry practice does not assume that the tilt axis is normal to the reflector dip. In this paper, we assign this tilt axis direction as a convenience for both wavefield modeling and separation filters computation). Therefore, in complex TI models, both the local anisotropy parameters ϵ and δ, and the local symmetry axes with tilt ν and azimuth α can be space-dependent.

This technique of separation by projecting the vector wavefields onto polarization vectors has been applied only to 2D VTI models (Dellinger 1991; Yan and Sava 2009) and for P-mode separation for 3D VTI models (Dellinger 1991). This technique is based on the plane-wave solution to the anisotropic elastic wave equation. For all modes, the plane-wave approximation yields linear polarization (which means that the polarization direction does not change with time) except at singularities. However, in fact, shear modes around the symmetry axis have non-linear polarizations, which cannot be characterized by the plane-wave asymptotic approximation. This problem is ameliorated in 2D because we assume that the SV mode is polarized in the 2D plane. For 3D models, the main challenge resides in the fact that we cannot obtain plane-wave solutions for fast and slow shear modes along singular directions. It is possible to apply the 2D separation method to 3D TTI models using the following procedure. First, project the elastic wavefields onto symmetry-axis planes (which contain P- and SV-modes) and the isotropy plane (which contains the SH-mode only); then separate P- and SV-modes in the symmetry-axis planes using divergence and curl operators for isotropic media or polarization vector projection for TI media. However, this approach is difficult as wavefields are usually constructed in Cartesian coordinates and symmetry-axis planes of the models are not aligned with the Cartesian coordinates. Furthermore, for heterogeneous models, the symmetry-axis planes change spatially, which makes projection of wavefields onto symmetry-axis planes impossible. To

avoid these problems, we propose a simpler and more straightforward solution to separate wave modes with 3D operators, which eliminates the need for projecting the wavefields onto symmetry-axis planes. The new approach constructs shear-wave filters by exploiting the mutual orthogonality of shear modes with the P mode, whose polarization vectors are computed by solving 3D Christoffel equations.

In this paper, we briefly review wave mode separation for symmetry-planes of VTI media and then we extend the algorithm to symmetry-axis planes of TTI media. Then, we generalize the wave mode separation to 3D TI media. Finally, we demonstrate wave mode separation in 2D with homogeneous and heterogeneous examples and separation in 3D with a homogeneous TTI example.

WAVE-MODE SEPARATION FOR 2D TRANSVERSE ISOTROPIC MEDIA

Wave-mode separation for symmetry-axis planes of vertical transverse isotropic media

Dellinger and Etgen (1990) separate P- and SV-modes in 2D VTI media by projecting the wavefields onto the directions in which P- and S-modes are polarized. For example, in the wavenumber domain, one can project the wavefields onto the P-wave polarization vectors $\mathbf{U}_P$ to obtain P-waves:

$$\widetilde{P} = i\,\mathbf{U}_P(\mathbf{k})\widetilde{\mathbf{W}} = i\,U_x\,\widetilde{W}_x + i\,U_z\,\widetilde{W}_z\,, \tag{1}$$

Here, $\widetilde{P}$ is the P-wave mode in the wavenumber domain, $\mathbf{k} = \{k_x, k_z\}$ is the wavenumber vector, $\widetilde{\mathbf{W}}$ is the elastic wavefield in the wavenumber domain and $\mathbf{U}_P(\mathbf{k})$ is the P-wave polarization vector as a function of the wavenumber $\mathbf{k}$.

The polarization vectors $\mathbf{U}$ ($\mathbf{k}$) of plane waves for VTI media in the symmetry-axis planes can be found by solving the Christoffel equation (Aki and Richards 2002; Tsvankin 2005):

$$\left[\mathbf{G} - \rho V^2\mathbf{I}\right]\mathbf{U} = 0\,, \tag{2}$$

where $\mathbf{G}$ is the Christoffel matrix with $G_{ij} = c_{ijkl}n_jn_l$, in which c_{ijkl} is the stiffness tensor. The vector $\mathbf{n} = \frac{\mathbf{k}}{|\mathbf{k}|}$ is the unit vector orthogonal to the plane wavefront, with n_j and n_l being the components in the j and l directions and the subscripts i, j, k, l range over 1,2,3. The eigenvalues V of this system correspond to the phase velocities of different wave modes and are dependent on the plane wave propagation direction $\mathbf{k}$. The Christoffel equation is an asymptotic solution to the elastic wave equation and is only exactly valid for homogeneous media. We use the solution here to obtain the plane-wave solution for media whose parameters do not vary spatially very fast.

For plane waves in the vertical symmetry-axis plane of a TTI medium, since P and SV modes are decoupled from the SH-mode and polarized in the symmetry-axis planes, one can set $n_y = 0$ and obtain

$$\begin{bmatrix} G_{11} - \rho V^2 & G_{12} \\ G_{12} & G_{22} - \rho V^2 \end{bmatrix} \begin{bmatrix} U_x \\ U_z \end{bmatrix} = 0\,, \tag{3}$$

where

$$G_{11} = c_{11}n_x^2 + c_{55}n_z^2\,, \tag{4}$$

$$G_{12} = (c_{13} + c_{55})\,n_xn_z\,, \tag{5}$$

$$G_{22} = c_{55}n_x^2 + c_{33}n_z^2\,. \tag{6}$$

Equation (3) allows one to compute the polarization vectors $\mathbf{U}_P = \{U_x, U_z\}$ and $\mathbf{U}_{SV} = \{-U_z, U_x\}$ (the eigenvectors of the matrix $\mathbf{G}$) given the stiffness tensor at every location of the medium.

Equation (1) represents the separation process for the P-mode in 2D homogeneous VTI media. To separate wave modes for heterogeneous models, one needs to use different polarization vectors at every location of the model (Yan and Sava 2009), because the polarization vectors change spatially with medium parameters. In the space domain, an expression equivalent to equation (1) at each grid point is

$$P = \nabla_a\,\mathbf{W} = L_x[W_x] + L_z[W_z]\,, \tag{7}$$

where $L[\,\cdot\,]$ indicates spatial filtering and L_x and L_z are the filters to separate P-waves representing the inverse Fourier transforms of iU_x and iU_z, respectively. The terms L_x and L_z define the 'pseudo-derivative operators' in the x and z directions for a VTI medium, respectively and they change according to the material parameters, V_{P0}, V_{S0}(V_{P0} and V_{S0} are the P and S velocities along the symmetry axis, respectively), ϵ and δ (Thomsen 1986).

Wave-mode separation for symmetry-axis planes of tilted transverse isotropic media

The separation algorithm for TTI models is similar to the approach used for VTI models. The main difference is that for VTI media, the wavefields consist of P- and SV-modes and equations (1) and (7) can be used for separation in all vertical planes of a VTI medium. However, for TTI media, this separation only works in the plane containing the normal of

the reflector, where P- and SV-waves are polarized, while other vertical planes contain SH-waves as well. Note that the 'SH-wave' is a term that was originally used in isotropic media to refer to a shear-wave polarized horizontally and perpendicular to the 2D reflection plane, in which the P-wave is polarized. We use the term 'SH-wave' in TI media as a shear-mode that is polarized perpendicular to the symmetry-axis plane. The SH-wave in TI media is not necessarily horizontal.

To obtain the polarization vectors for P- and S-modes in the symmetry-axis planes of TTI media, one needs to solve for the Christoffel equation (3) with

$$G_{11} = c_{11}n_x^2 + 2c_{15}n_x n_z + c_{55}n_z^2\,, \tag{8}$$

$$G_{12} = c_{15}n_x^2 + (c_{13} + c_{55})\,n_x n_z + c_{35}n_z^2\,, \tag{9}$$

$$G_{22} = c_{55}n_x^2 + 2c_{35}n_x n_z + c_{33}n_z^2\,. \tag{10}$$

Here, since the symmetry axis of the TTI medium is not aligned with the vertical axis k_z, the TTI Christoffel matrix is different from its VTI equivalent. The stiffness tensor is determined by the parameters V_{P0}, V_{S0}, ϵ, δ and the tilt angle ν.

In anisotropic media, $\mathbf{U}_P$ generally deviates from the wave vector direction $\mathbf{k} = \frac{\omega}{V}\mathbf{n}$, where ω is the angular frequency and V is the phase vector. Figure 1(a,b) shows the P-mode polarization in the wavenumber domain for a VTI medium and a TTI medium with a 30° tilt angle, respectively. The polarization vectors for the VTI medium deviate from radial directions, which represent the isotropic polarization vectors $\mathbf{k}$. The polarization vectors of the TTI medium are rotated 30° about the origin from the vectors of the VTI medium.

Figure 2(a,b) shows the components of the P-wave polarization vectors of a VTI medium and a TTI medium with a 30° tilt angle, respectively. Figure 2(c) shows that the polarization vectors in Fig. 2(b) rotated to the symmetry axis and its orthogonal direction of the TTI medium. Comparing Figs 2(a) and 2(c), we see that within the circle that has a radius of the Nyquist wavenumber, the components of this TTI medium are rotated 30{°} from those of the VTI medium. However, note that the z and x components of the polarization vectors for the VTI medium (Fig. 2a) are symmetric with respect to the x and z axes, respectively; in contrast, the vectors of the TTI medium (Fig. 2c) are not symmetric because the symmetry axis is not aligned with the z-axis of the Cartesian system.

To maintain continuity at the negative and positive Nyquist wavenumbers for Fourier transform to obtain space-domain filters, i.e. at $k_x, k_z = \pm\pi$ radians, one needs to apply tapers to the vector components. For VTI media, a taper corresponding to the function (Yan and Sava 2009)

$$f(k) = -\frac{8\sin(k)}{5k} + \frac{2\sin(2k)}{5k} - \frac{8\sin(3k)}{105k} + \frac{\sin(4k)}{140k}, \tag{11}$$

can be applied to the x and z components of the polarization vectors (Fig. 2a), where k represent the components k_x and k_z of the vector $\mathbf{k}$. This taper ensures that U_x and U_z are zero at $k_z = \pm\pi$ radians and $k_x = \pm\pi$ radians, respectively. The

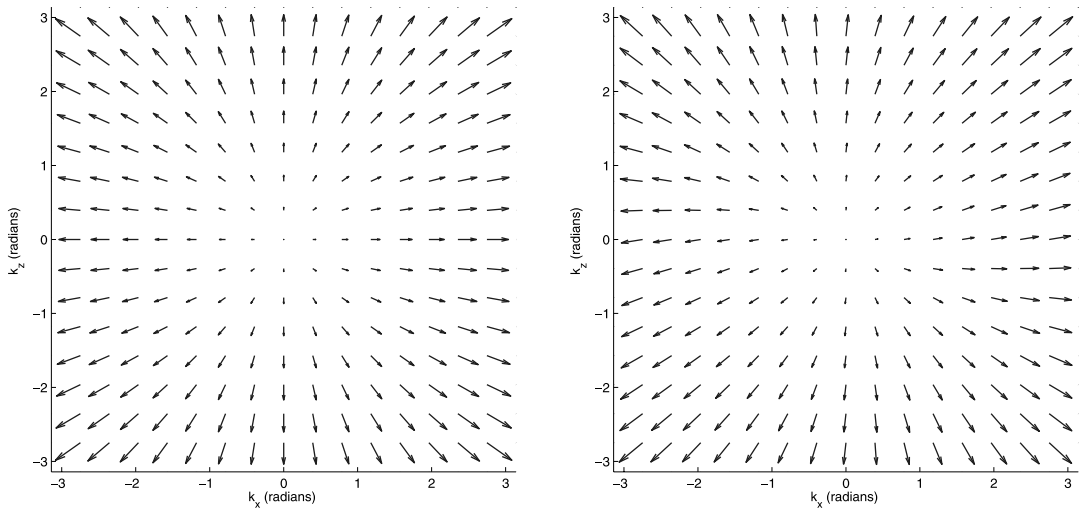


Figure 1 Polarization vectors of P-mode as a function of normalized wavenumbers k_x and k_z ranging from $-\pi$ radians to $+\pi$ radians, for a) a VTI model with $V_{P0} = 3.0$ km/s, $V_{S0} = 1.5$ km/s, $\epsilon = 0.25$ and $\delta = -0.29$ and for b) a TTI model with the same model parameters as (a) and a symmetry axis tilt $\nu = 30°$. The vectors in (b) are rotated 30° with respect to the vectors in (a) around $k_x = 0$ and $k_z = 0$.

components U_x and U_z are continuous in the z and x directions across the Nyquist wavenumbers, respectively, due to the symmetry of the VTI media. Moreover, the application of this taper transforms polarization vector components to 8th order centred derivatives. If the components of the isotropic polarization vectors $\mathbf{k}$ are tapered by the function in equation (11) and then transformed to the space domain, one obtains the conventional 8th order centered finite-difference derivative operators $\frac{\partial}{\partial x}$ and $\frac{\partial}{\partial z}$ (Yan and Sava 2009). Therefore, the VTI separators reduce to conventional derivatives – the components of the divergence and curl operators – when the medium is isotropic.

For TTI media, due to the asymmetry of the Fourier domain derivatives (Fig. 2b), one needs to apply a rotational symmetric taper to the polarization vector components to obtain continuity across Nyquist wavenumbers. A simple Gaussian taper

$$g(\mathbf{k}) = C \exp\left[-\frac{|\mathbf{k}|^2}{2\sigma^2}\right], \tag{12}$$

can be used, where C is a normalizing constant. When one chooses a standard deviation of $\sigma = 1$ radian, the magnitude of this taper at $|\mathbf{k}| = \pi$ radians is about 0.7% of the peak value and therefore the TTI components can be safely assumed to be continuous across the Nyquist wavenumbers. Tapering the polarization vector components in Fig. 2 with the function in equation (12), one obtains the plots in Fig. 3. The panels in Fig. 3, which exhibits circular continuity across the Nyquist wavenumbers, transform to the space-domain separators in Fig. 4. The space-domain filters for TTI media are rotated from the VTI filters, also by the tilt angle ν.

The value of σ determines the size of the operators in the space domain and also affects the frequency content of the separated wave modes. For example, Fig. 5 shows the component U_z and operator L_z for σ values of 0.25, 1.00 and 1.25 radians. A larger value of σ results in more concentrated operators in the space domain and better preserved frequency of the separated wave modes. However, one needs to ensure that the function $g(\mathbf{k})$ at $|\mathbf{k}| = \pi$ radians is small enough to assume continuity of the value function across Nyquist wavenumbers. When one chooses $\sigma = 1$ radian, the TTI components can be safely assumed to be continuous across the Nyquist wavenumbers.

For heterogeneous models, we can pre-compute the polarization vectors at each grid point as a function of the V_{P0}/V_{S0} ratio, the Thomsen parameters ϵ and δ and tilt angle ν. We then transform the tapered polarization vector components to the space domain to obtain the spatially-varying separators L_x and L_z. The separators for the entire model are stored and used to separate P- and S-modes from reconstructed elastic wavefields at different time steps. Thus, wavefield separation in TI media can be achieved simply by non-stationary filtering with spatially varying operators. We assume that the medium parameters vary slowly in space and that they are locally homogeneous. For complex media, the localized operators behave similarly to the long finite-difference operators used for finite-difference modeling at locations where medium parameters change rapidly. The computational issues of the wave mode separation will be discussed later in the paper.

WAVE-MODE SEPARATION FOR 3D TRANSVERSE ISOTROPIC MEDIA

In order to separate all three modes, P, SV and SH, one needs to construct 3D separators. Dellinger (1991) shows that P-waves can be separated from two shear modes by a straightforward extension of the 2D algorithm. Indeed, for 3D TI media, one can always obtain the P-mode by constructing P-wave separators represented by the polarization vector $\mathbf{U}_P = \{U_x, U_y, U_z\}$ and then projecting the 3D elastic wavefields onto the vector $\mathbf{U}_P$. The P-wave polarization vector with components $\{U_x, U_y, U_z\}$ is obtained by solving the 3D Christoffel matrix (Aki and Richards 2002; Tsvankin 2005):

$$\begin{bmatrix} G_{11}-\rho V^2 & G_{12} & G_{13} \\ G_{12} & G_{22}-\rho V^2 & G_{23} \\ G_{13} & G_{23} & G_{33}-\rho V^2 \end{bmatrix} \begin{bmatrix} U_x \\ U_y \\ U_z \end{bmatrix} = 0\,. \tag{13}$$

The notations in this equation have the same definitions as in equation (2). For TTI media, the matrix $\mathbf{G}$ has the elements

$$\begin{aligned} G_{11} = {} & c_{11}n_x^2 + c_{66}n_y^2 + c_{55}n_z^2 + 2c_{16}n_xn_y \\ & + 2c_{15}n_xn_z + 2c_{56}n_yn_z\,, \end{aligned} \tag{14}$$

$$\begin{aligned} G_{22} = {} & c_{66}n_x^2 + c_{22}n_y^2 + c_{44}n_z^2 + 2c_{26}n_xn_y \\ & + (c_{45}+c_{46})n_xn_z + 2c_{24}n_yn_z\,, \end{aligned} \tag{15}$$

$$\begin{aligned} G_{33} = {} & c_{55}n_x^2 + c_{44}n_y^2 + c_{33}n_z^2 + 2c_{45}n_xn_y \\ & + 2c_{35}n_xn_z + 2c_{34}n_yn_z\,, \end{aligned} \tag{16}$$

$$\begin{aligned} G_{12} = {} & c_{16}n_x^2 + c_{26}n_y^2 + c_{45}n_z^2 + (c_{12}+c_{66})n_xn_y \\ & + (c_{14}+c_{56})n_xn_z + (c_{25}+c_{46})n_yn_z\,, \end{aligned} \tag{17}$$

$$\begin{aligned} G_{13} = {} & c_{15}n_x^2 + c_{46}n_y^2 + c_{35}n_z^2 + (c_{14}+c_{56})n_xn_y \\ & + (c_{13}+c_{55})n_xn_z + (c_{36}+c_{45})n_yn_z\,, \end{aligned} \tag{18}$$

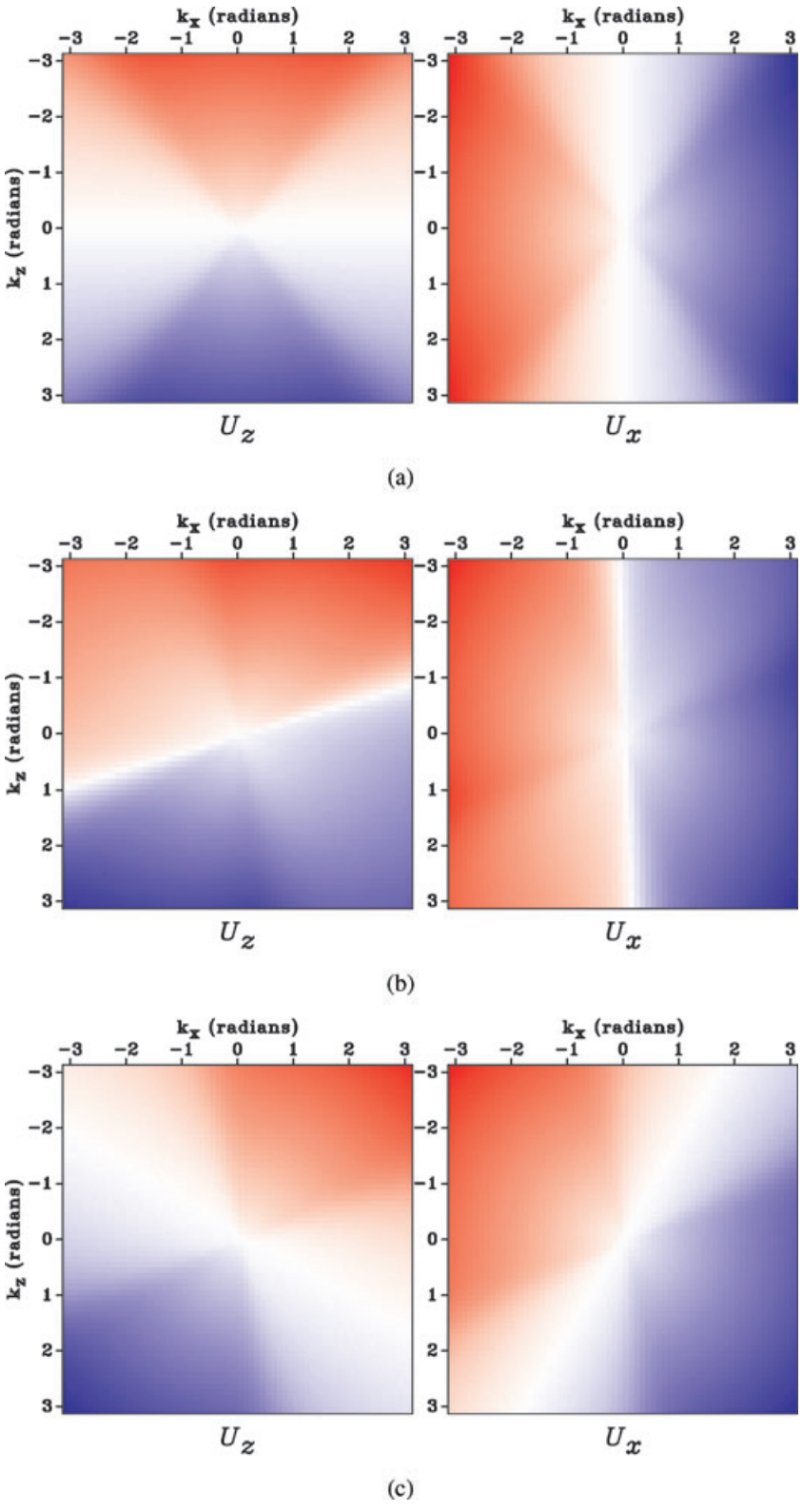


Figure 2 Z and x components of the polarization vectors for P-mode in the Fourier domain for a) a VTI medium with $\epsilon = 0.25$ and $\delta = -0.29$ and for b) a TTI medium with $\epsilon = 0.25$, $\delta = -0.29$, and $\nu = 30^\circ$. Panel (c) represents the projection of the polarization vectors shown in (b) onto the tilt axis and its orthogonal direction.

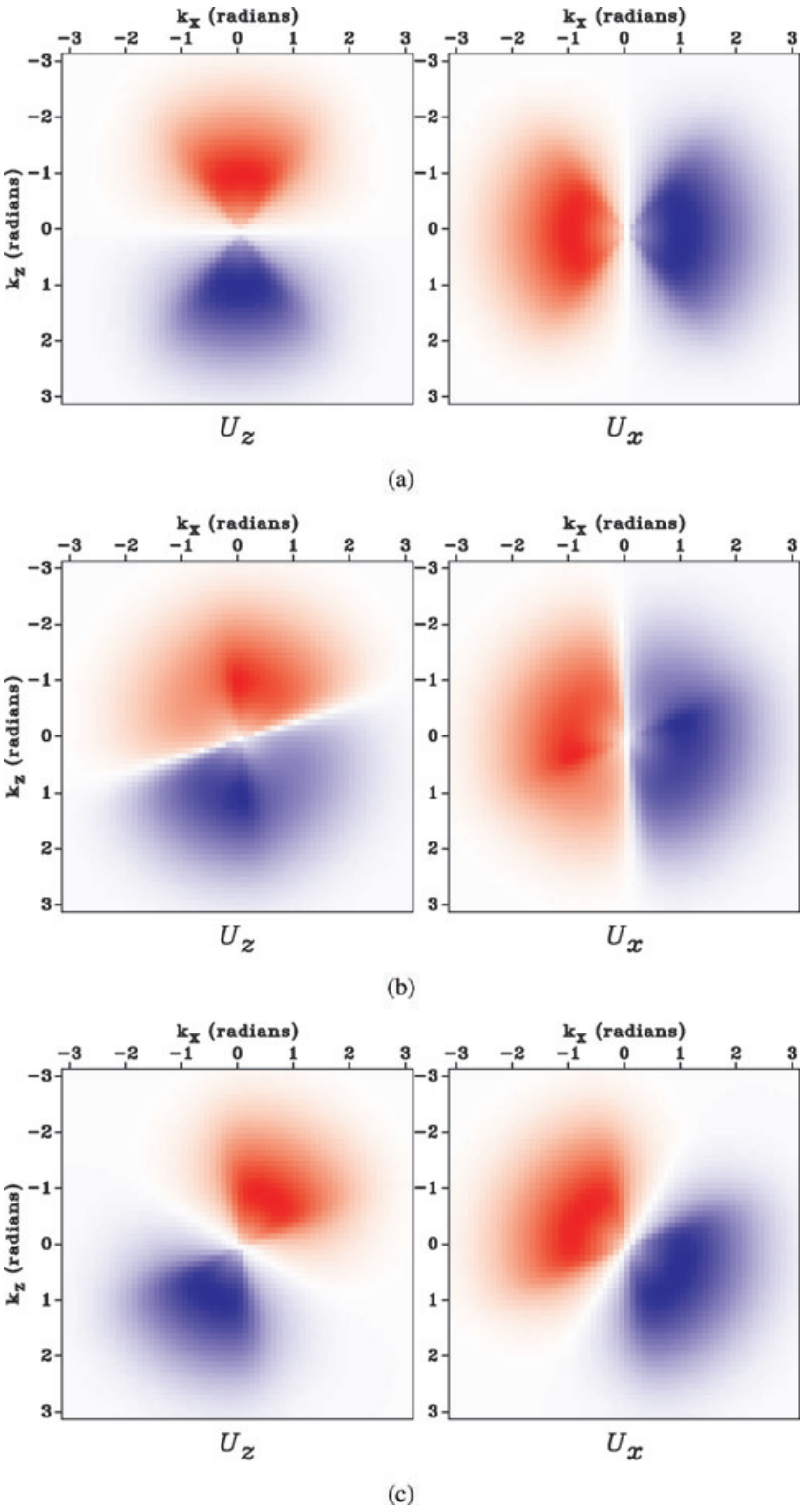


Figure 3 Wavenumber-domain vectors in Fig. 2 are tapered by the function in equation (12) to avoid Nyquist discontinuity. Panel (a) corresponds to Fig. 2(a), panel (b) corresponds to Fig. 2(b) and panel (c) corresponds to Fig. 2(c).

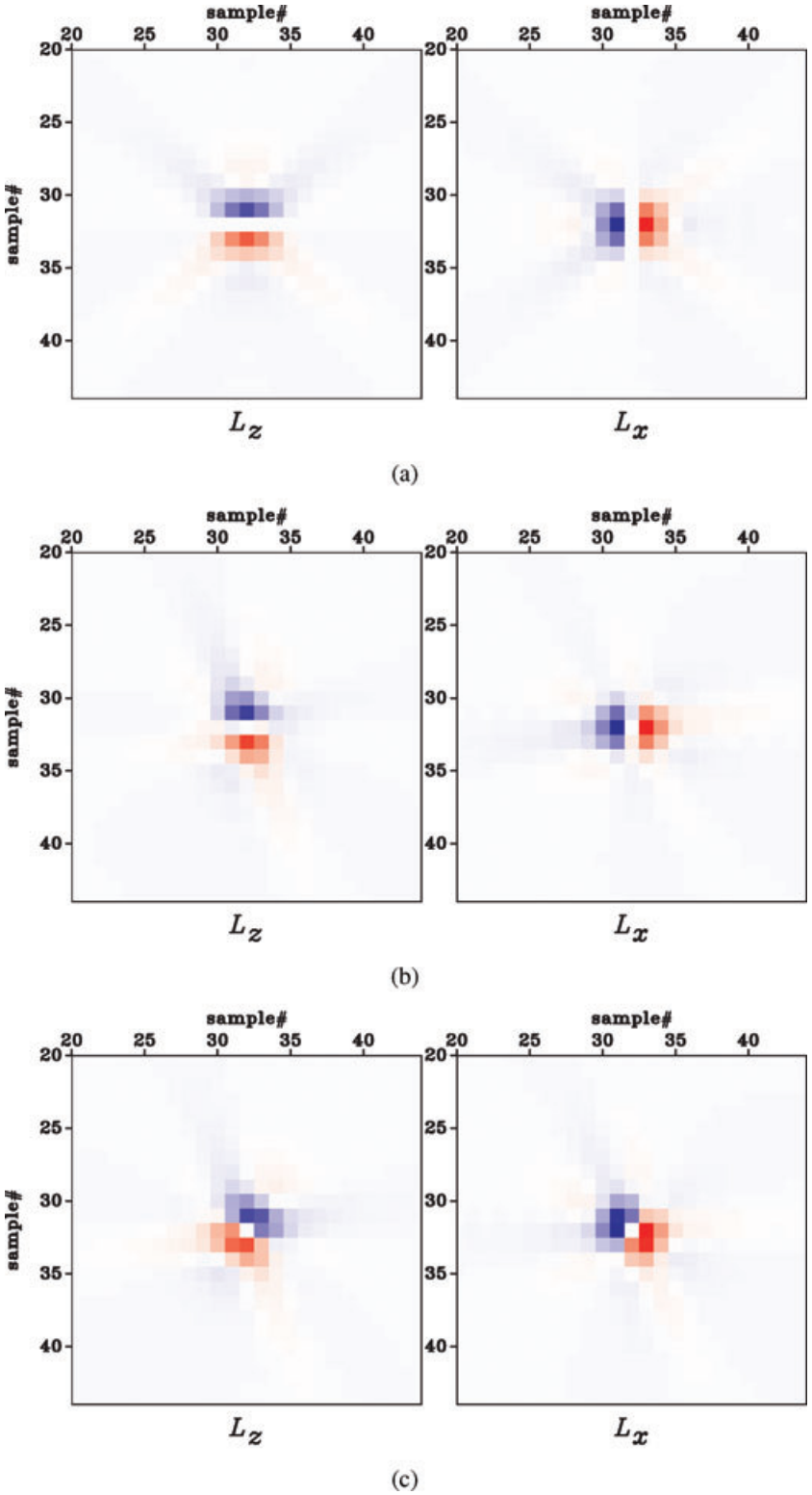


Figure 4 Space-domain wave-mode separators for the medium shown in Fig. 1. They are the Fourier transformation of the polarization vectors shown in Fig. 3. Panel (a) corresponds to Fig. 3(a), panel (b) corresponds to Fig. 3(b) and panel (c) corresponds to Fig. 3(c). The zoomed views show 24×24 samples out of the original 64×64 samples around the center of the filters.

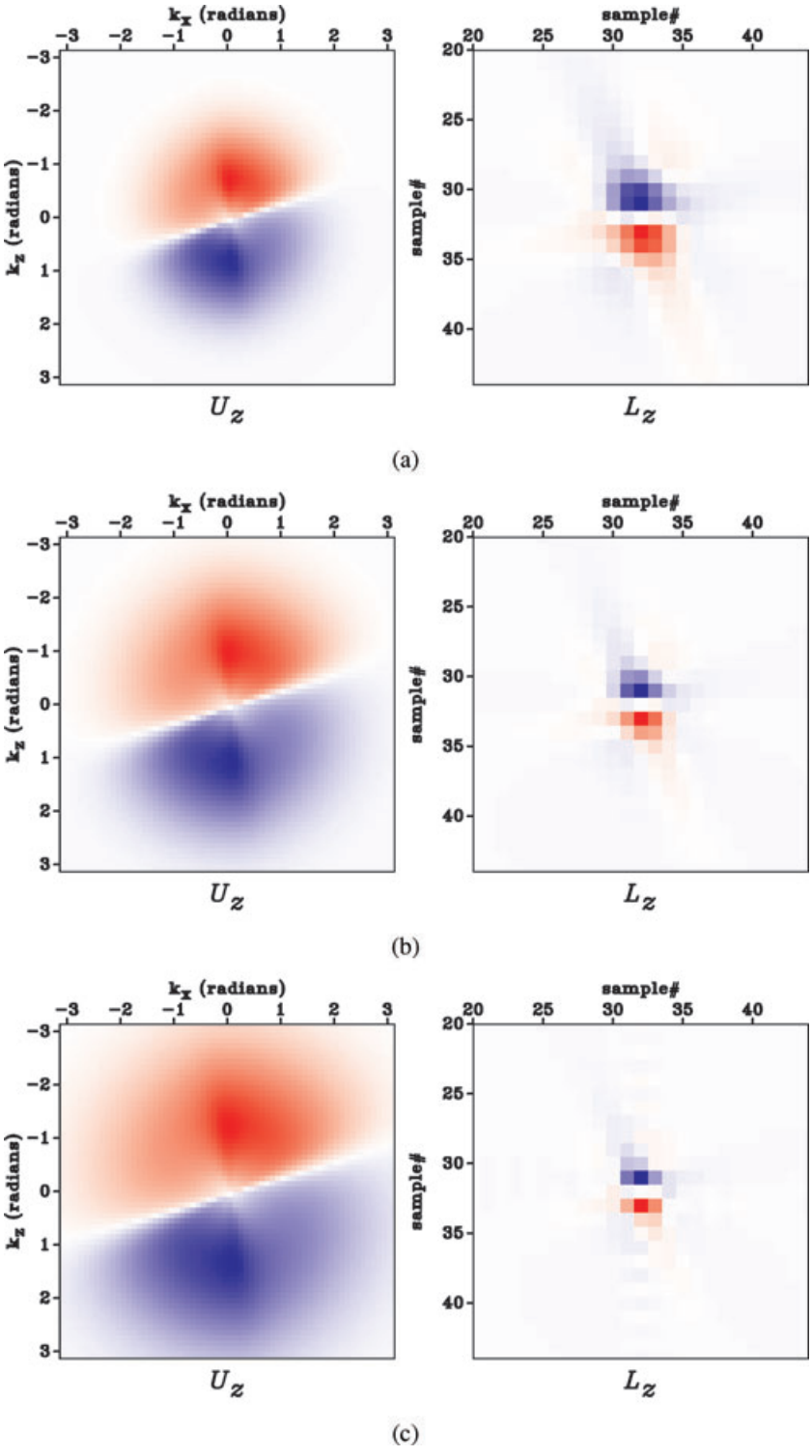


Figure 5 Panels (a)–(c) correspond to component U_z (left) and operator L_z (right) for σ values of 0.25, 1.00, and 1.25 radians in equation (12), respectively. A larger value of σ results in more spread components in the wavenumber domain and more concentrated operators in the space domain.

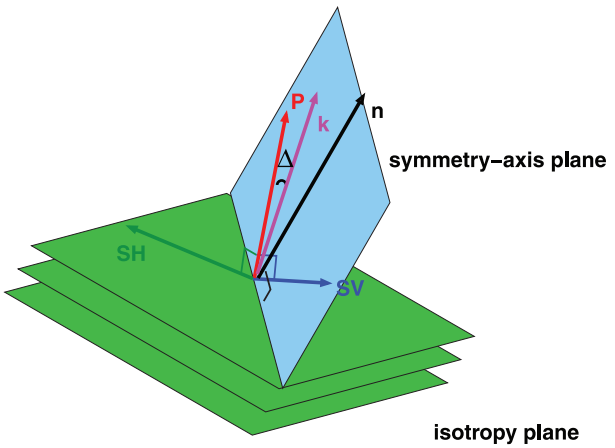


Figure 6 Schematic showing the elastic wave-modes polarization in a 3D TI medium. The three parallel planes represent the isotropy planes of the medium. The vector **n** represents the symmetry axis, which is orthogonal to the isotropy plane. The vector **k** is the propagation direction of a plane wave. The wave-modes P, SV and SH are polarized in the direction **P**, **SV** and **SH**, respectively. The three modes are polarized orthogonal to each other.

$$G_{23} = c_{56}n_x^2 + c_{24}n_y^2 + c_{34}n_z^2 + (c_{25} + c_{46})n_x n_y + (c_{36} + c_{45})n_x n_z + (c_{23} + c_{44})n_y n_z\,. \tag{19}$$

When constructing shear mode separators, one faces an additional complication: SV- and SH-waves have the same velocity along the symmetry axis of a TI medium and this singularity prevents one from obtaining polarization vectors for shear modes in this particular direction by solving the Christoffel equation (Tsvankin 2005). In 3D TI media, the polarization of the shear modes excited by point sources are non-linear around the singular directions and cannot be characterized by a plane-wave solution (Vavryčuk 1999). Consequently, constructing 3D global separators for fast and slow shear modes is difficult.

To mitigate the effects of this 'kiss' singularity, we use the mutual orthogonality among the P, SV and SH modes depicted in Fig. 6. In this figure, vector $\mathbf{n} = \{\sin\nu\cos\alpha,\ \sin\nu\sin\alpha,\ \cos\nu\}$ represents the symmetry axis of a TTI medium, with ν and α being the tilt and azimuth of the symmetry axis, respectively. The wave vector **k** characterizes the propagation direction of a plane wave. Vectors **P**, **SV** and **SH** symbolize the compressional and fast and slow shear polarization directions, respectively. For TI media, the symmetry axis **n** and any wave vector **k** (which does not coincide with **n**) form a symmetry-axis plane. For a plane wave propagating in the direction **k**, the P-wave is polarized in this symmetry-axis plane and deviates from the vector **k**; the SV- and SH-waves are polarized perpendicular to the P-mode, in and out of the symmetry-axis plane, respectively. The only exception to this definition is in the symmetry-axis direction, where vectors **n** and **k** coincide. Although **n** and **k** do not form a plane in this singular direction, the SV and SH waves can still be defined mathematically the same way.

Using this mutual orthogonality among all three modes, we first obtain the SH-wave polarization vector $\mathbf{U}_{SH}$ by cross multiplying vectors **n** and **k**, which ensures that the SH mode is polarized orthogonal to symmetry-axis planes:

$$\mathbf{U}_{SH} = \mathbf{n}\times\mathbf{k} = \begin{bmatrix} k_z n_y - k_y n_z \\ k_x n_z - k_z n_x \\ k_y n_x - k_x n_y \end{bmatrix}. \tag{20}$$

Then we calculate the SV polarization vector $\mathbf{U}_{SV}$ by cross multiplying polarization vectors P and SH modes, which ensures the orthogonality between SV and P modes and SV and SH modes:

$$\mathbf{U}_{SV} = \mathbf{U}_P \times \mathbf{U}_{SH} = \begin{bmatrix} k_y n_x U_y - k_x n_y U_y + k_z n_x U_z - k_x n_z U_z \\ k_z n_y U_z - k_y n_z U_z + k_x n_y U_x - k_y n_x U_x \\ k_x n_z U_x - k_z n_x U_x + k_y n_z U_y - k_z n_y U_y \end{bmatrix}. \tag{21}$$

Here, the magnitude of the P-wave polarization vectors for a certain wavenumber $|\mathbf{k}|$ is a constant:

$$|U_P| = \sqrt{U_x^2 + U_y^2 + U_z^2} = c\,. \tag{22}$$

This ensures that for a certain wavenumber, P-waves obtained by projecting the elastic wavefields onto the polarization vectors are uniformly scaled. For comparison, the magnitudes of all three modes are respectively

$$|U_P| = c\,, \tag{23}$$

$$|U_{SV}| = c\sin\phi\,, \tag{24}$$

$$|U_{SH}| = c\sin\phi\,, \tag{25}$$

where ϕ is the polar angle of the propagating plane wave, i.e., the angle between vectors **k** and **n**. Figure 7 shows the polarization vectors of P-, SH-, and SV-modes computed using equations (13), (20 and (21), respectively. The P-wave polarization vectors in Fig. 7(a) all have the same magnitude, but the SV and SH polarization vectors in Figs 7(c) and 7(b) do not. In the symmetry axis direction, they are zero vectors and in the isotropy plane, they are unit vectors. The amplitudes and directions of the shear-mode polarization vectors in the **k**-domain change smoothly. Using separators represented by solutions to equation (13) and expressions (20) and (21) to

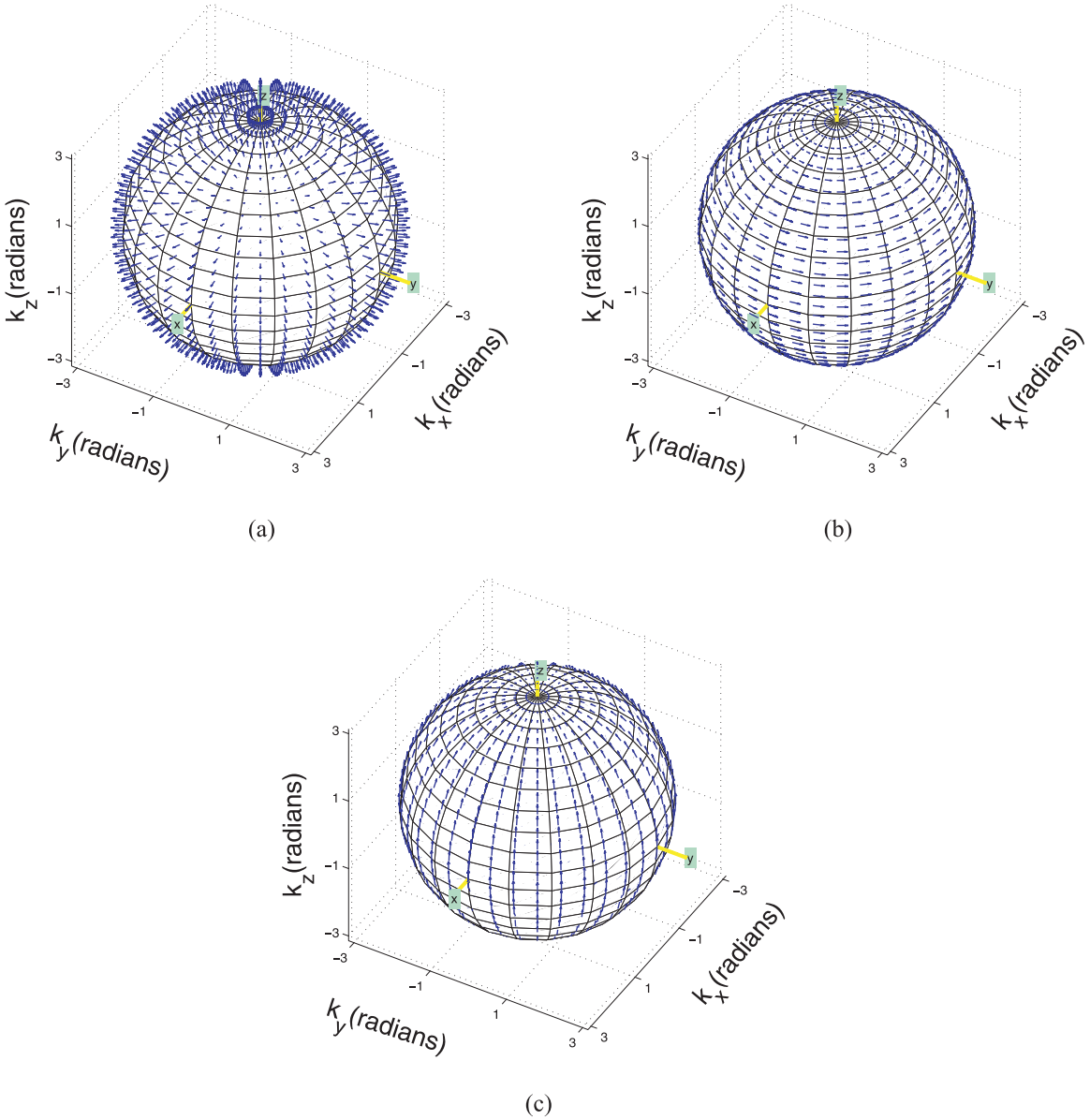


Figure 7 Wave-mode polarization for P-, SH- and SV-mode for a VTI medium with parameters $V_{P0} = 4.95$ km/s, $V_{S0} = 2.48$ km/s, $\epsilon = 0.4$ and $\delta = 0.1$. The P-mode polarization is computed using the 3D Christoffel equation and SV and SH polarizations are computed using equations (21) and (20). Note that the SV- and SH-wave polarization vectors have zero amplitude in the vertical direction.

filter the wavefields, we obtain separated shear modes that are scaled differently than the P-mode. For a certain wavenumber, the shear modes are scaled by sin ϕ, with ϕ being the polar angle, which increases from zero in the symmetry direction to unity in the orthogonal directions. Physically, S-wave polarizations in the symmetry direction are determined by the source. However, to simplify the problem, the shear-waves around the singularity are zeroed.

The components of the polarization vectors for P-, SV- and SH-waves can be transformed back to the space domain to construct spatial filters for 3D heterogeneous TI media. For example, Fig. 8 illustrates nine spatial filters transformed from the Cartesian components of the polarization vectors shown in Fig. 7. All these filters can be spatially varying when the medium is heterogeneous. Therefore, in principle, wave mode separation in 3D would perform well even for models that

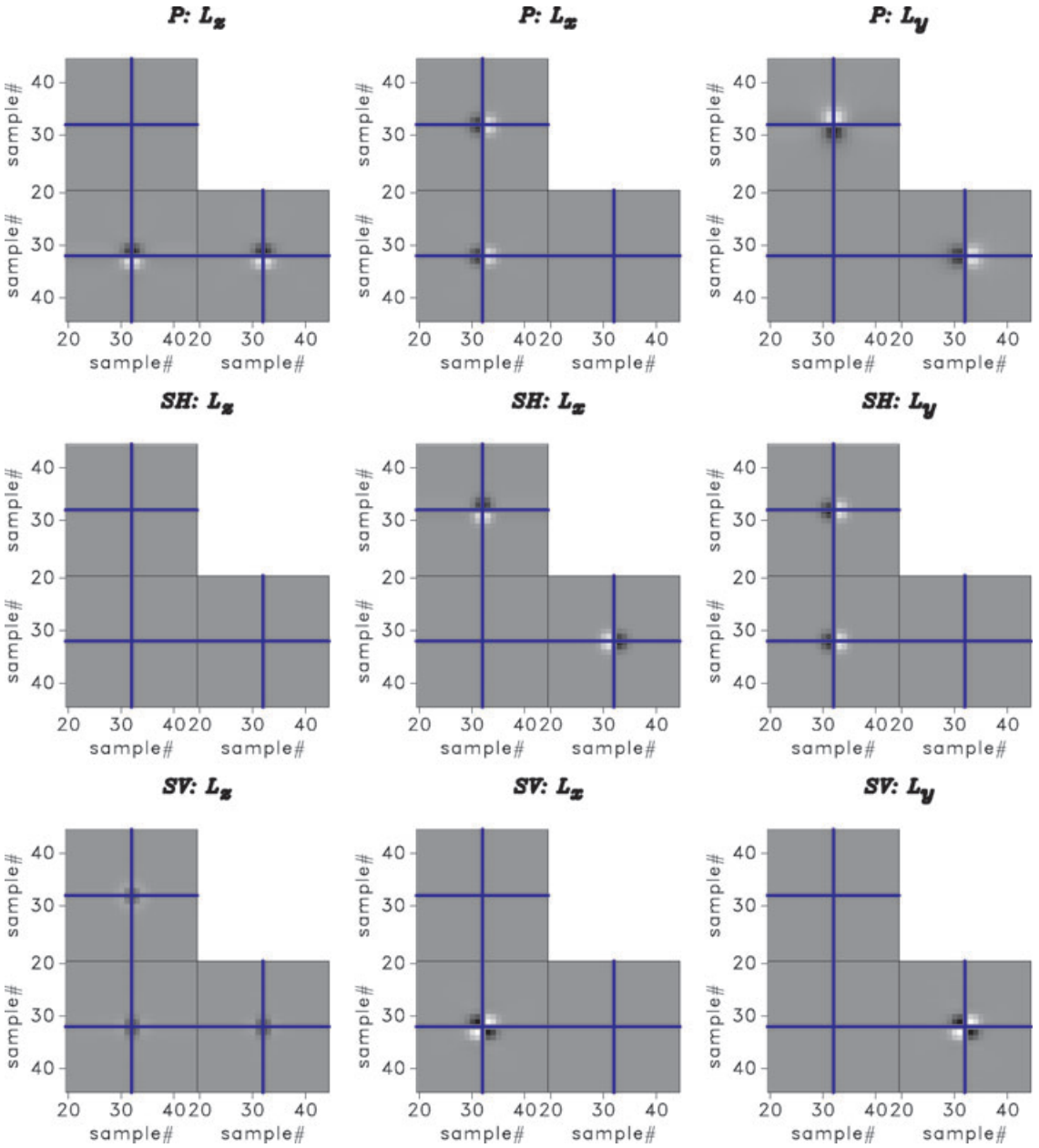


Figure 8 Separation filters L_x, L_y and L_z for the P, SV and SH modes for a VTI medium. The corresponding wavenumber-domain polarization vectors are shown in Fig. 7. Note that the filter L_z for the SH mode is blank because the z component of the polarization vector is zero. The zoomed views show 24 × 24 samples out of the original 64 × 64 samples around the center of the filters.

have complex structures and arbitrary tilts and azimuths of TI symmetry.

EXAMPLES

We illustrate the anisotropic wave mode separation with a simple fold synthetic example and a more challenging model based on the elastic Marmousi II model (Bourgeois *et al.* 1991). We then show the wave-mode separation for a 3D TTI model.

2D tilted transverse isotropic fold model

Consider the 2D fold model shown in Fig. 9. Panels 9(a) and 9(b) show V_{P0} and the local tilts ν of the model, respectively. Parameters V_{S0}, ϵ, δ and density have linear relations with

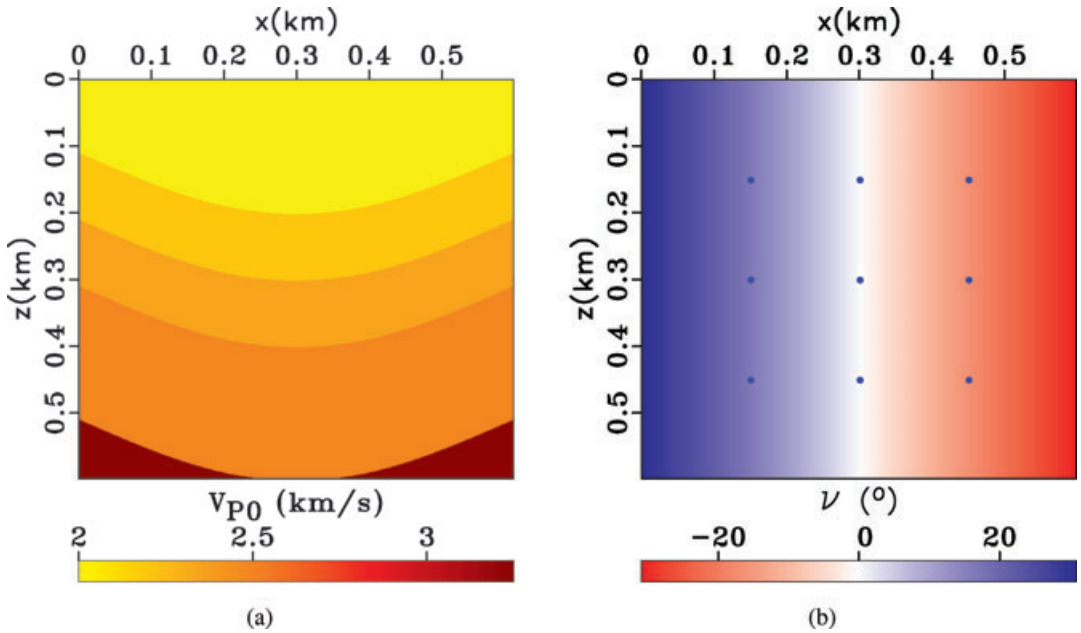


Figure 9 Fold model with parameters a) V_{P0} and b) tilt angle ν. The dots in panel (b) correspond to the locations of the anisotropic operators shown in Fig. 10.

the P-wave velocity V_{P0}. The symmetry axis is orthogonal to the reflectors throughout the model. Figure 10 illustrates the separators obtained at different locations in the model and defined by the intersections of x coordinates 0.15, 0.3, 0.45 km and z coordinates 0.15, 0.3, 0.45 km, shown by the dots in Fig. 9(b). Since the operators correspond to different combinations of the V_{P0}/V_{S0} ratio and parameters ϵ, δ, and tilt angle ν, they have different forms. However, the orientation of the operators conform to the corresponding tilts at the locations shown by the dots in Fig. 9(b). For complex models, the symmetry axes vary spatially, which makes it difficult to rotate the wavefields to the local symmetry axis directions. Consequently, the elastic wavefields are reconstructed in untilted Cartesian coordinates and when separating wave modes, we use operators constructed in conventional Cartesian coordinates. To illustrate the relationship between the operators and the local tilts, the filters in Fig. 10 are projected onto the local symmetry axes and the orthogonal directions at the filter location. As shown in Fig. 4, the rotated filters (Fig. 4c) show a clearer relation with the tilt angle, while the non-rotated filters (Fig. 4b), which are used in the wave mode separation, do not.

Figure 11(a) shows the vertical and horizontal components of one snapshot of the simulated elastic anisotropic wavefield; Fig. 11(b) shows the separation into P- and S-modes using divergence and curl operators; Fig. 11(c) shows the separation into P and S modes using VTI filters, i.e., assuming zero tilt throughout the model; and Fig. 11(d) shows the separation obtained with the TTI operators constructed using the local medium parameters with correct tilts. The isotropic separation shown in Fig. 11(b) is incomplete; for example, at $x = 0.4$ km and $z = 0.1$ km and at $x = 0.4$ km and $z = 0.35$ km, residuals for direct P and S arrivals are visible in the P and S panels, respectively. A comparison of Figs 11(c) and 11(d) indicates that the spatially-varying derivative operators with correct tilts successfully separate the elastic wavefields into P- and S-modes, while the VTI operators only work in the part of the model that is locally VTI.

Marmousi II model

Our second model (Fig. 12) uses an elastic anisotropic version of the Marmousi II model (Bourgeois *et al.* 1991). In the modified model, V_{P0} is taken from the original model (Fig. 12a), the V_{P0}/V_{S0} ratio ranges from 2–2.5, and the density ρ is taken from the original model. The parameter ϵ and δ are derived from the density model ρ with the relations of $\epsilon = 0.25\rho - 0.3$ and $\epsilon = 0.125\rho - 0.1$, respectively. The parameter ϵ ranges from 0.13–0.36, and parameter δ ranges from 0.11–0.24. These anisotropy parameters are obtained by assuming linear relationships to the density models and therefore, they both follow the structure of the model.

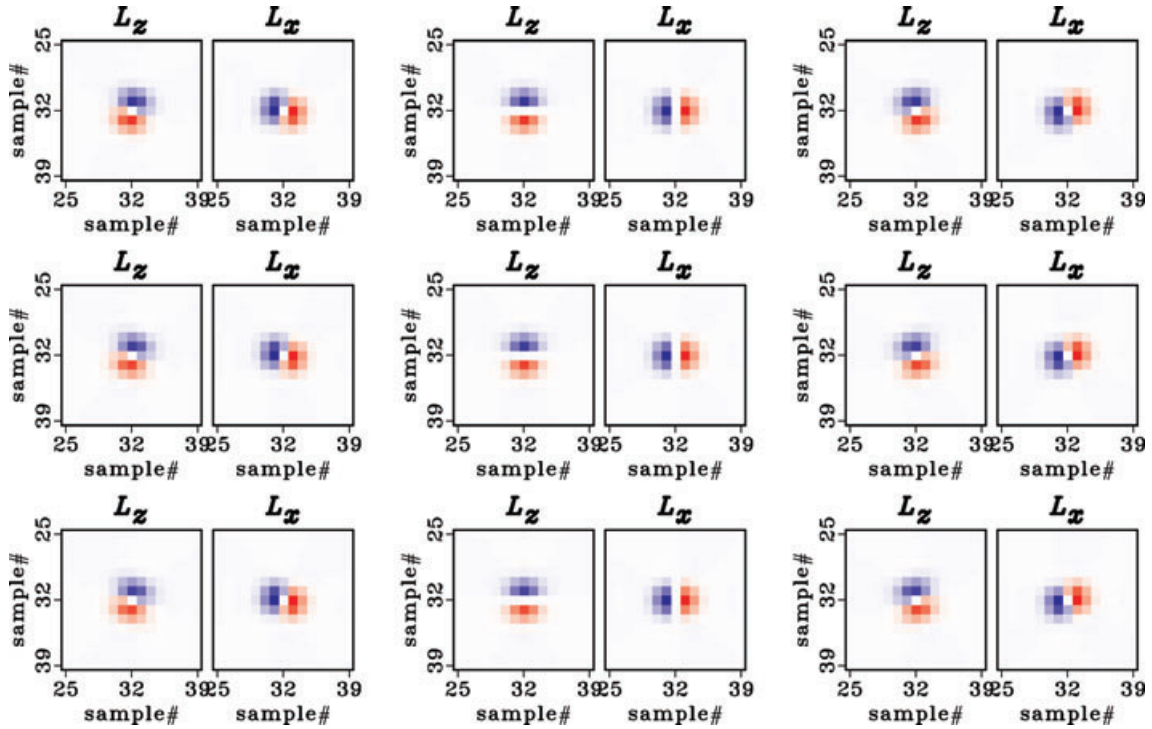


Figure 10 TTI wave-mode separation filters projected to local symmetry axes and their orthogonal directions. Here, we use $\sigma = 1$ in equation (12) to taper the polarization vector components before the Fourier transform. The filters correspond to the intersections of $x = 0.15$, 0.3, 0.45 km and $z = 0.15$, 0.3, 0.45 km for the model shown in Fig. 9. The locations of these operators are also shown by the dots in Fig. 9(b). The filters in these panels are zoomed view of 15×15 samples out of the original 64×64 samples around the center.

Figure 12(b) represents the local dips obtained from the density model using plane wave destruction filters (Fomel 2002). The dip model is used to simulate the wavefields and also used to construct TTI separators. A displacement source oriented at 45° to the vertical direction and located at coordinates $x = 11$ km and $z = 1$ km is used to simulate the elastic anisotropic wavefield.

Figure 13(a) presents one snapshot of the simulated elastic wavefields using the anisotropic model shown in Fig. 12. Figures 13(b), 13(c) and 13(d) demonstrate the separation using conventional divergence and curl operators, VTI filters and correct TTI filters, respectively. The VTI filters are constructed assuming zero tilt throughout the model and the TTI filters are constructed with the dips used for modeling. As expected, the conventional divergence and curl operators fail at locations where anisotropy is strong. For example, in Fig. 13(b) at coordinates $x = 12.0$ km and $z = 1.0$ km strong S-wave residual exists and at coordinates $x = 13.0$ km and $z = 1.5$ km a strong P-wave residual exists. VTI separators fail at locations where the dip and, therefore, the symmetry-axis tilt, is large. For example, in Fig. 13(c) at coordinates $x = 10.0$ km and $z = 1.2$ km, there are strong S-wave residuals. However, even for this complicated model, separation using TTI separators is effective at locations where medium parameters change rapidly.

3D tilted transverse isotropic model

We use a homogeneous TTI model to illustrate the separation of P-, SV- and SH-modes. Figure 14 shows a snapshot of the elastic wavefields in the z, x and y directions. A displacement source located at the centre of the model and oriented at tilt 45° and azimuth 45° is used to excite the wavefield. Figure 15 shows successfully separated P-, SV- and SH-modes. In this model, the parameter γ, which characterizes the anisotropy of SH-mode, is set to zero so that the SH-mode propagation is isotropic. For this homogeneous model, a spherical wavefront in the SH-panel indicates successful separation of SV- and SH-modes.

Because this model is homogeneous, the separation is implemented in the wavenumber domain to reduce computation cost. For heterogeneous models, 3D non-stationary filtering is necessary to separate different wave modes. We do not perform wave mode separation in 3D heterogeneous models

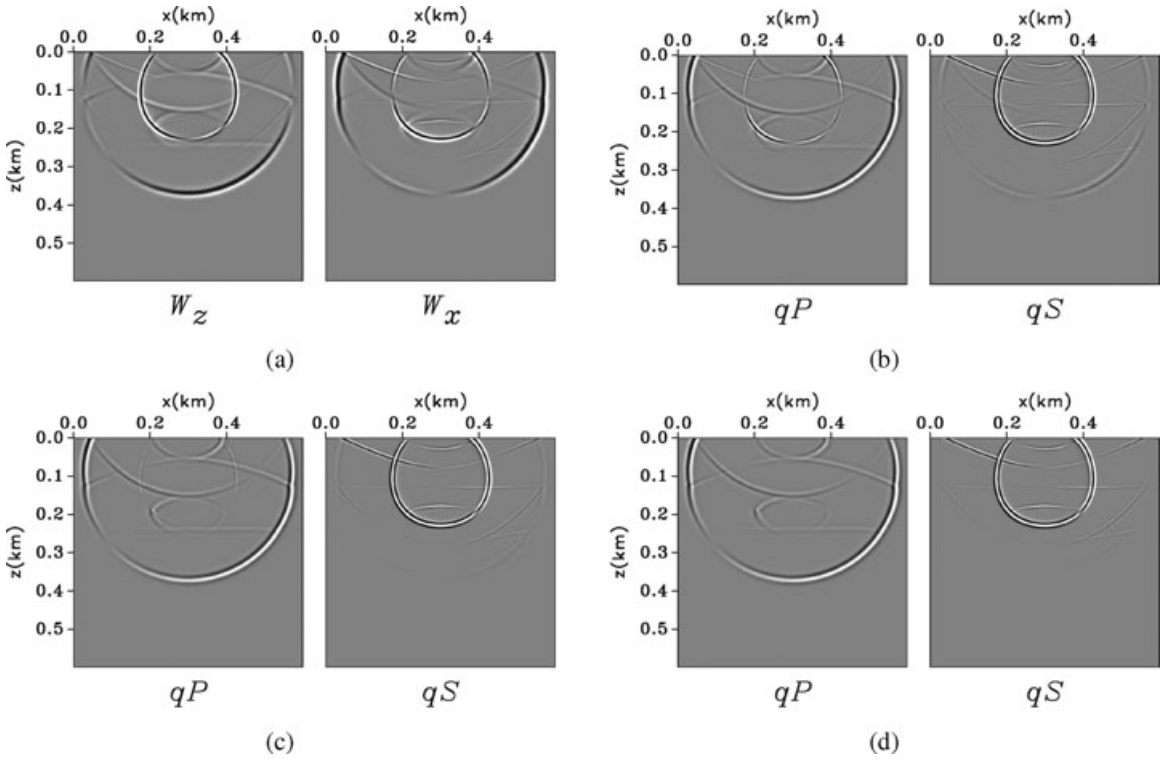


Figure 11 (a) A snapshot of the anisotropic wavefield simulated with a vertical point displacement source at $x = 0.3$ km and $z = 0.1$ km for the model shown in Fig. 9. Panels (b) to (d) are the anisotropic P- and S-modes separated using isotropic, VTI and TTI separators, respectively. The separation is incomplete in panels (b) and (c) where the model is strongly anisotropic and where the model tilt is large, respectively. Panel (d) shows the best separation among all.

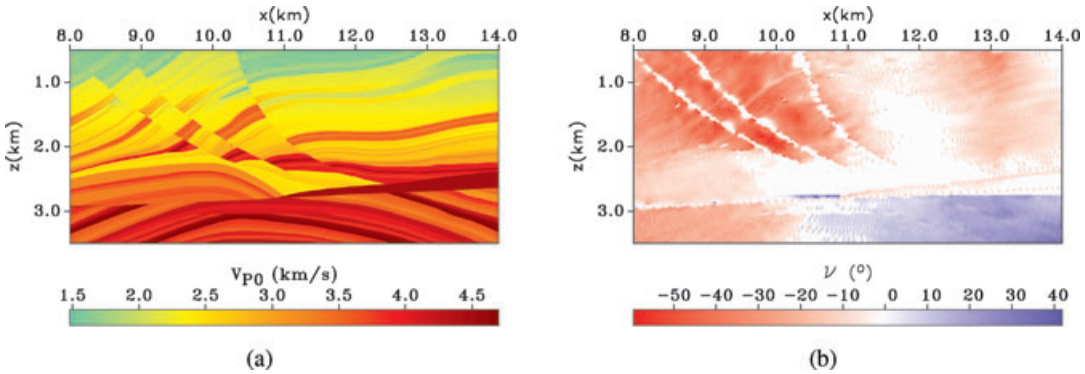


Figure 12 Anisotropic elastic Marmousi II model with a) V_{P0} b) local tilt angle ν.

because of the high computational cost, as will be discussed in more detail in the following section.

DISCUSSION

Computational issues

The separation of wave modes for heterogeneous TI models requires non-stationary spatial filtering with large operators (operators of 50 samples in each dimension are used in this paper), which is computationally expensive. The cost is directly proportional to the size of the model and to the size of each operator. Furthermore, in a simple implementation, the storage for the separation operators of the entire model is proportional to the size of the model and to the size of each operator. Suppose that a 3D elastic TTI model is characterized by model parameters V_{P0}, V_{S0}, ϵ, δ and symmetry axis

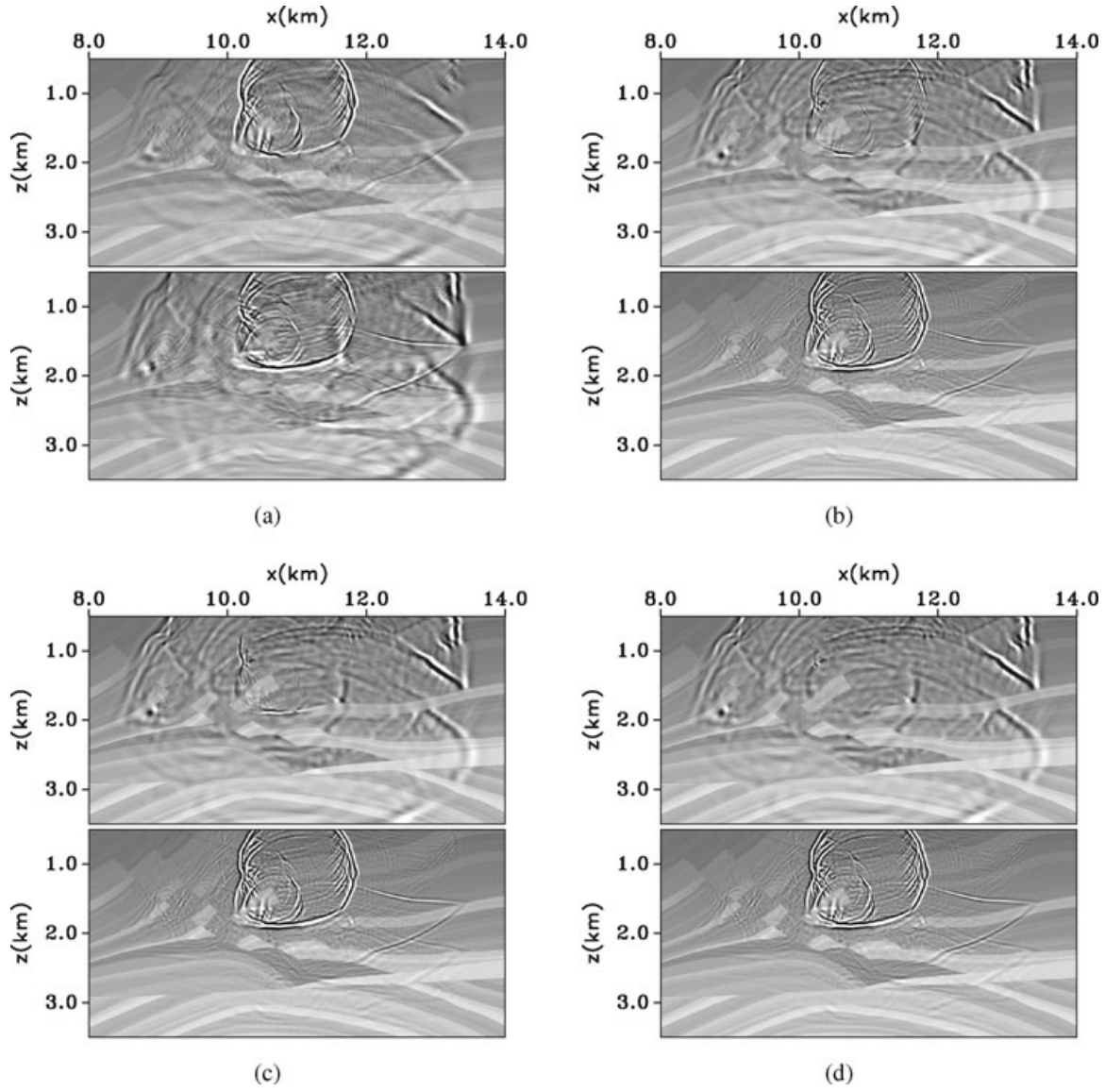


Figure 13 (a) A snapshot of the vertical and horizontal displacement wavefield simulated for model shown in Fig. 12. Panels (b) to (d) are the P- and SV-wave separation using $\nabla \cdot$ and $\nabla \times$, VTI separators, and TTI separators, respectively. The separation is incomplete in panels (b) and (c) where the model is strongly anisotropic and where the model tilt is large, respectively. Panel (d) shows the best separation among all.

tilt angle ν and azimuth angle α. For a 3D model of 300 $\times$ 300 $\times$ 300 grid points, if one assumes that all operators have a size of 50 $\times$ 50 $\times$ 50 samples, the storage for the operators is 300^3 grid points $\times$ 50^3 samples/independent operator $\times$ 3 independent operators/grid point $\times$ 4 Bytes/sample =40.5 TB. This is not feasible in ordinary processing. However, since there are relatively few medium parameters (i.e., the V_{P0}/V_{S0} ratio, ϵ, δ and angles ν and α), which determine the properties of the operators, one can construct a look-up table of operators as a function of these parameters, and search the appropriate operators at every location in the model when doing wave mode separation. For example, suppose one knows that $V_{P0}/V_{S0} \in [1.5, 2.0]$, $\epsilon \in [0, 0.3]$, $\delta \in [0, 0.1]$, the symmetry axis tilt $\nu \in [-90^\circ, 90^\circ]$ and azimuth $\alpha \in [-180^\circ, 180^\circ]$, one can sample the V_{P0}/V_{S0} ratio at every 0.1, ϵ and δ at every 0.03 and the angles at every 15°. In this case, one only needs a storage of 6 $\times$ 10 $\times$ 3 $\times$ 12 $\times$ 24 combinations of medium parameters $\times$ 50^3 sample/independent

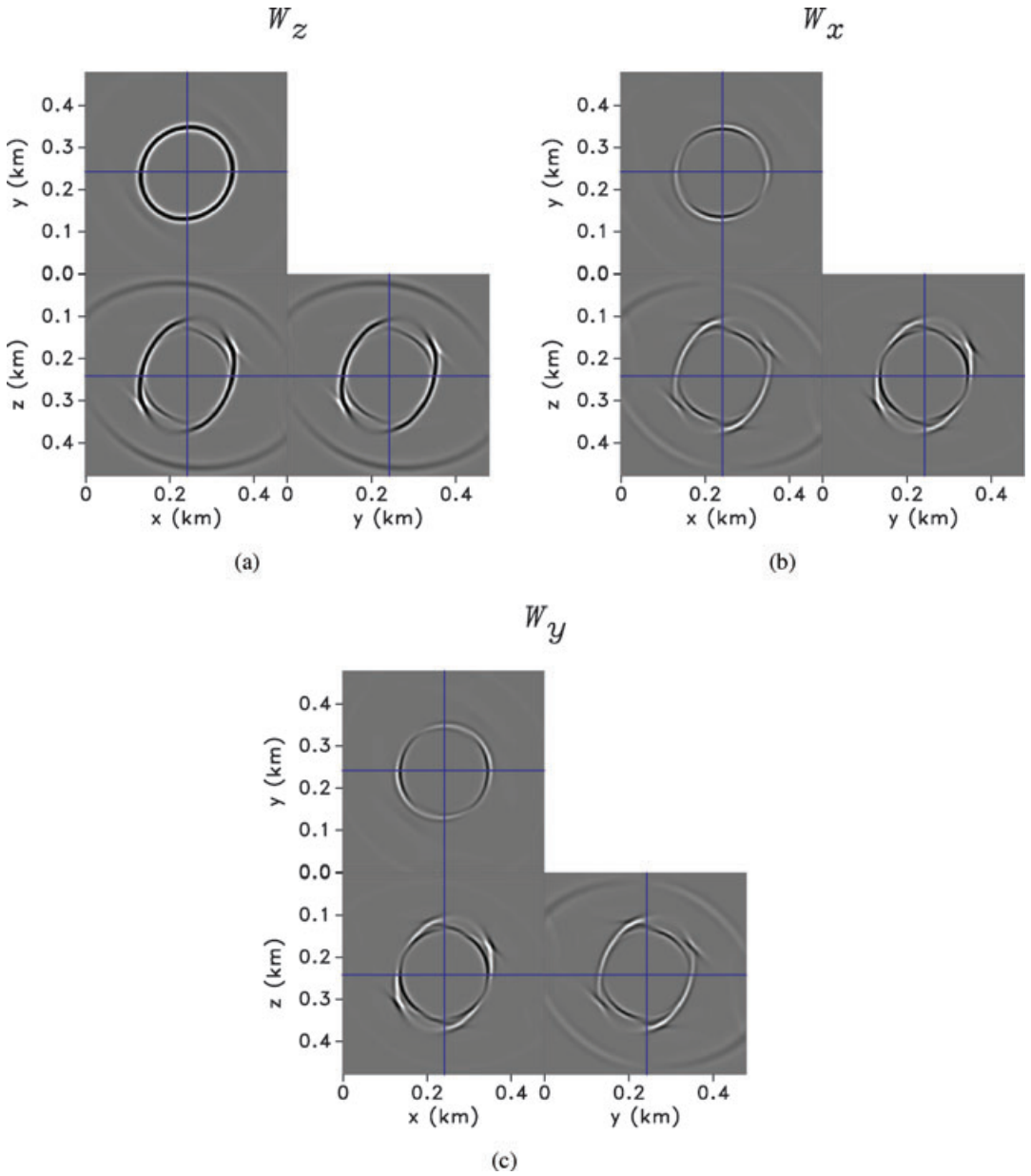


Figure 14 A snapshot of the elastic wavefield in the z, x and y directions for a 3D TTI model. The model has parameters $V_{P0} = 3.5$ km/s, $V_{S0} = 1.75$ km/s, $\rho = 2.0$ g/cm^3, $\epsilon = 0.4$, $\delta = 0.1$, and $\gamma = 0.0$. A displacement source oriented at 45° to the vertical direction and located at coordinates $x = 11$ km and $z = 1$ km is used to simulate the elastic anisotropic wavefield.

operator × 3 independent operators/combination of medium parameters × 4 Bytes/sample = 77 GB; this is more manageable, although still a large volume to store.

S wave-mode amplitudes

Although the procedure used in this paper to separate S-waves into SV- and SH- modes is straightforward, the amplitudes of S-modes are not accurate because the S-wave separators are not normalized for any given wavenumbers. The amplitudes of S-modes obtained in this way are zero in the symmetry-axis direction and gradually increase to unity in the isotropy plane.

The main problem that prevents one from constructing the 3D global shear wave separators is that the SV and SH polarization vectors are singular in the symmetry-axis direction,

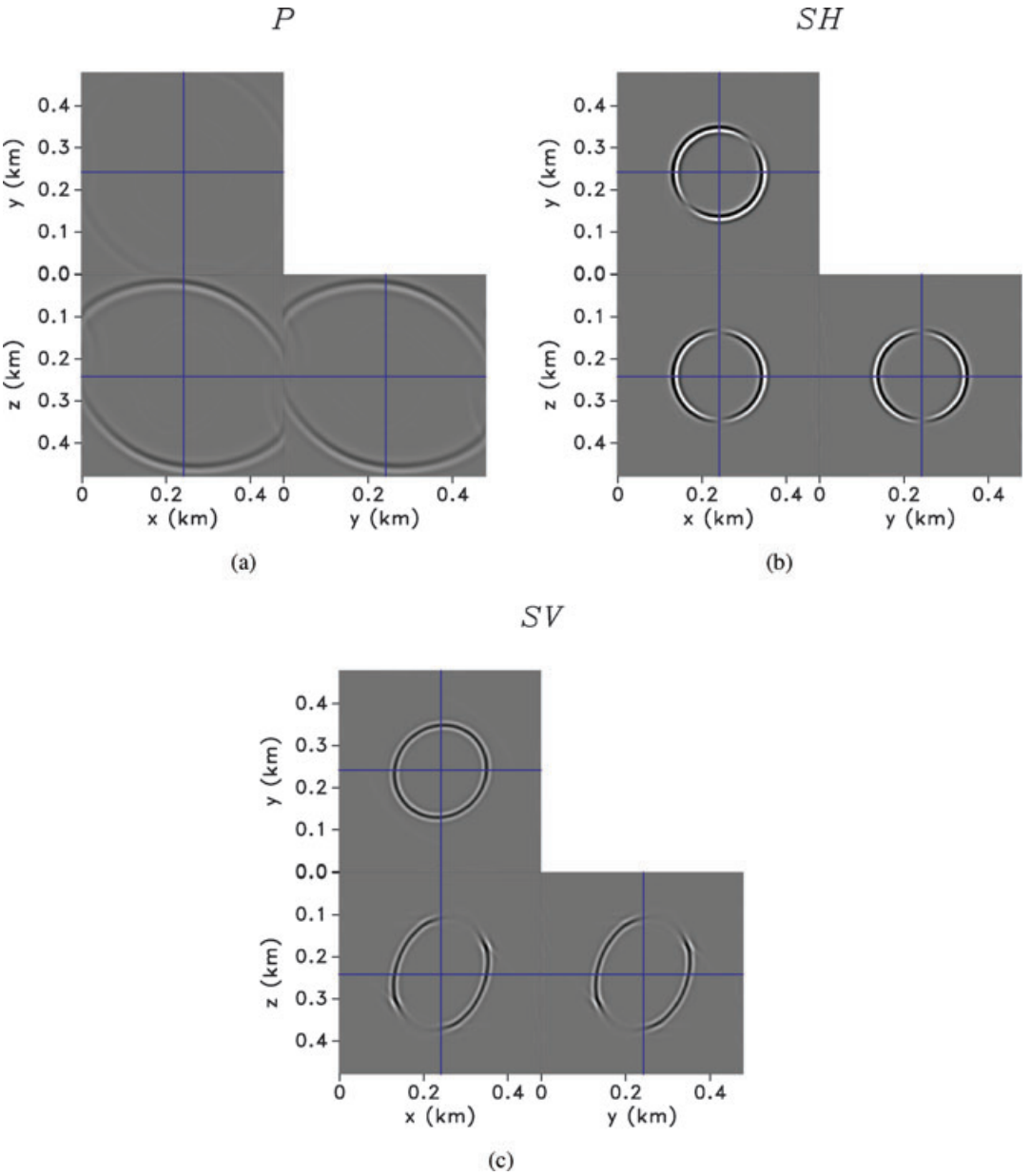


Figure 15 Separated P-, SV- and SH-wave-modes for the elastic wavefields shown in Fig. 14. P, SV, and SH are well separated from each other.

i.e., they are not defined by the plane-wave solution of the TI elastic wave equation. Various studies (Kiselev and Tsvankin 1989; Vavryčuk 1999; Tsvankin 2005) show that S-waves excited by point forces can have non-linear polarization in several special directions. For example, around the direction of point force, the S-wave can have non-linear polarization. This phenomenon exists even in isotropic media. Anisotropic velocity and amplitude variations can also cause the S-waves to be polarized non-linearly. For instance, S-wave triplication, S-wave singularities and S-wave velocity extrema can all result in S-wave polarization anomalies. In these special directions, SV- and SH-mode polarizations are incorrectly defined by the plane-wave theory. One possibility for obtaining more accurate S-wave amplitudes is to approximate the anomalous polarization with the major axes of the quasi-ellipses of the S-wave polarization, which can be obtained by incorporating the first-order term in the ray tracing method. This extension is impractical and remains outside the scope of this paper.

Although the simplified approach used in this paper ignores the complicated polarization behaviour in some propagation directions, it does successfully separate fast and slow shear modes kinematically. This allows one to use the separated scalar shear-modes for implementing the subsequent imaging condition and obtain images with clear physical meaning. However, one should be cautious while trying to use the separated shear modes for true amplitude imaging or amplitude versus angle interpretations. Further correction might be for necessary for these amplitude related studies.

CONCLUSIONS

Different wave modes in elastic media can be separated by projecting the vector wavefields onto the polarization vectors of each mode. For heterogeneous models, it is necessary to separate wave modes in the space domain by non-stationary filtering. We present a method for obtaining spatially-varying wave mode separators for TI models, which can be used to separate elastic wave modes in complex media. The method computes the components of the polarization vectors in the wavenumber domain and then transforms them to the space domain to obtain spatially-varying filters. In order for the operators to work in TI models with a tilted symmetry axis, we incorporate one more parameter – the local tilt angle ν – in addition to the parameters needed for the VTI operators. These kind of spatial filters can be used to separate complicated wavefields in TI models with strong heterogeneity and anisotropy. We test the separation with synthetic models that have realistic geologic complexity. The results support the effectiveness of wave mode separation with non-stationary filtering.

We also extend the wave mode separation to 3D TI models. The separation of three modes in 3D TI media is based on the plane-wave solution to the elastic wave equation. The P-mode separators can be constructed by solving the Christoffel equation for the P-wave eigenvectors with local medium parameters. The SV and SH separators are constructed using the mutual orthogonality among P, SV and SH modes. For the three modes, there are a total number of nine separators, with three components for each mode. The separators vary with the medium parameters V_{P0}, V_{S0}, ϵ, δ and tilt ν and azimuth α of the symmetry axis. In anisotropic media, P-waves polarize more linearly than S-waves. Therefore, the plane-wave approximation preserves the separated P-waves better than the S-waves. Nevertheless, the proposed technique successfully separates fast and slow shear wavefields. The process of constructing 3D separators and separating wave modes in 3D eliminates the step of projecting the wavefields into the symmetry-axis plane and isotropy plane, which is only effective for models with an invariant symmetry axis. Spatially-varying 3D separators have potential benefits for complex models and can be used to separate wave modes in elastic reverse time migration for TTI models. The spatially-varying 3D separators require a large computational and storage cost and therefore, a more efficient separation method, such as the proposed table look-up alternative, is necessary for a successful implementation.

ACKNOWLEDGEMENTS

We acknowledge the financial support of the sponsors of the Center for Wave Phenomena at Colorado School of Mines. The authors would like to thank Paul Fowler and two anonymous reviewers for their thorough reviews, which greatly improved the manuscript. The reproducible numeric examples in this paper use the Madagascar open-source software package freely available from http://www.reproducibility.org.

REFERENCES

Aki K. and Richards P. 2002. *Quantitative Seismology*, 2nd edn. University Science Books.

Alkhalifah T. and Sava P. 2010. A transversely isotropic medium with a tilted symmetry axis normal to the reflector. *Geophysics* **75**, A19–A24.

Bourgeois A., Bourget M., Lailly P., Poulet M., Ricarte P. and Versteeg R. 1991. The Marmousi experience. In: *The Marmousi Experience, Proceedings of the 1990 EAEG Workshop, Marmousi, Model and Data* (eds R. Versteeg and G. Grau), pp. 5–16.

Charles S., Mitchell D.R., Holt R.A., Lin J. and Mathewson J. 2008. Data-driven tomographic velocity analysis in tilted transversely isotropic media: A 3D case history from the Canadian foothills. *Geophysics* **73**, VE261–VE268.

Dellinger J. 1991. *Anisotropic seismic wave propagation*. PhD thesis, Stanford University.

Dellinger J. and Etgen J. 1990. Wave-field separation in two-dimensional anisotropic media (short note). *Geophysics* **55**, 914–919.

Fomel S. 2002. Applications of plane-wave destruction filters. *Geophysics* **67**, 1946–1960.

Fowler P.J., Du X. and Fletcher R.P. 2010. Coupled equations for reverse time migration in transversely isotropic media. *Geophysics* **75**, S11–S22.

Godfrey R.J. 1991. Imaging canadian foothills data. 61st SEG meeting, Houston, Texas, USA, Expanded Abstracts, 207–209.

Kiselev A.P. and Tsvankin I. 1989. A method of comparison of exact and asymptotic wave field computations. *Geophysical Journal International* **96**, 253–258.

Stewart R.R., Gaiser J., Brown R.J. and Lawton D.C. 2003. Converted-wave seismic exploration: Applications. *Geophysics* **68**, 40–57.

Sun R., McMechan G.A., Hsiao H. and Chow J. 2004. Separating P- and S-waves in prestack 3D elastic seismograms using divergence and curl. *Geophysics* **69**, 286–297.

Thomsen L. 1986. Weak elastic anisotropy. *Geophysics* **51**, 1954–1966.

Tsvankin I. 2005. *Seismic Signatures and Analysis of Reflection Data in Anisotropic Media*, 2nd edn. Elsevier.

Vavryčuk V. 1999. Properties of S-waves near a kiss singularity: a comparison of exact and ray solutions. *Geophysical Journal International* **138**, 581–589.

Yan J. and Sava P. 2008. Isotropic angle-domain elastic reverse-time migration. *Geophysics* **73**, S229–S239.

Yan J. and Sava P. 2009. Elastic wave-mode separation for VTI media. *Geophysics* **74**, WB19–WB32.

Zhang Y. and Zhang H. 2009. A stable TTI reverse time migration and its implementation. 79th SEG meeting, Houston, Texas, USA, Expanded Abstracts, 2794–2798.